Conformational Changes in the α-Subunit Coupled to Binding of the β_2-Subunit of Tryptophan Synthase from *Escherichia coli*: Crystal Structure of the Tryptophan Synthase α-Subunit Alone[†,‡]

Kazuya Nishio,[§] Yukio Morimoto,[||,⊥] Manabu Ishizuka,[@] Kyoko Ogasahara,[§] Tomitake Tsukihara,[§] and Katsuhide Yutani*[,⊥]

Institute for Protein Research, Osaka University, 3-2 Yamadaoka, Suita, Osaka 565-0871, Japan, Research Reactor Institute, Kyoto University, Kumatori-cho, Sennan-gun, Osaka 590-0494, Japan, Department of Biological Science and Technology, Faculty of Engineering, The University of Tokushima, 2-1 Minamijosanjima-cho, Tokushima 770-8506, Japan, and RIKEN Harima Institute, 1-1-1 Kouto, Mikazuki-cho, Sayo-gun, Hyogo 679-5148, Japan

Received September 24, 2004; Revised Manuscript Received November 9, 2004

ABSTRACT: When the tryptophan synthase α- and β_2-subunits combine to form the $\alpha_2\beta_2$-complex, the enzymatic activity of each subunit is stimulated by 1−2 orders of magnitude. To elucidate the structural basis of this mutual activation, it is necessary to determine the structures of the α- and β-subunits alone and together with the $\alpha_2\beta_2$-complex. The crystal structures of the tryptophan synthase $\alpha_2\beta_2$-complex from *Salmonella typhimurium* (*St*$\alpha_2\beta_2$-complex) have already been reported. However, the structures of the subunit alone from mesophiles have not yet been determined. The structure of the tryptophan synthase α-subunit alone from *Escherichia coli* (*Ec*α-subunit) was determined by an X-ray crystallographic analysis at 2.3 Å, which is the first report on the subunits alone from the mesophiles. The biggest difference between the structures of the *Ec*α-subunit alone and the α-subunit in the *St*$\alpha_2\beta_2$-complex (*St*α-subunit) was as follows. Helix 2′ in the *St*α-subunit, including an active site residue (Asp60), was changed to a flexible loop in the *Ec*α-subunit alone. The conversion of the helix to a loop resulted in the collapse of the correct active site conformation. This region is also an important part for the mutual activation in the *St*$\alpha_2\beta_2$-complex and interaction with the β-subunit. These results suggest that the formation of helix 2′ that is essential for the stimulation of the enzymatic activity of the α-subunit is constructed by the induced-fit mode involved in conformational changes upon interaction between the α- and β-subunits. This also confirms the prediction of the conformational changes based on the thermodynamic analysis for the association between the α- and β-subunits.

The biological events in living cells are achieved by specific protein−protein or protein−ligand interactions. In many cases, the enzymatic activity and biological function of proteins are regulated upon formation of a high-order protein complex or binding of ligands. Allosteric control of the enzymatic activity is a typical example. The mode of protein−protein or protein−ligand interaction is divided into three different concepts as follows (*1*): "lock and key", originally introduced by E. Fischer in 1894, "induced fit" (*2*−*6*), and "pre-existing equilibrium hypothesis" (*7*, *8*). For these concepts, the structural changes in proteins are considered to be connected with the regulation of function.

As an ideal system for investigating the protein−protein interaction and ligand-mediated allosteric regulation, bacterial tryptophan synthase has been widely studied using genetic, biochemical, and kinetic methods (*9*−*16*). Tryptophan synthase catalyzes the last two steps in the biosynthesis of L-tryptophan. The bacterial enzyme is a multifunctional $\alpha_2\beta_2$-complex composed of nonidentical α- and β-subunits. The isolated α- and β_2-subunits catalyze different reactions, α- and β-reactions, respectively (eqs 1 and 2, respectively). The physiologically important reaction is the $\alpha\beta$-reaction (eq 3) catalyzed by the $\alpha_2\beta_2$-complex.

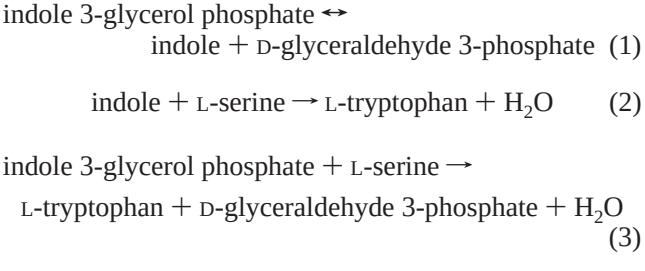

When the α- and β_2-subunits combine to form the $\alpha_2\beta_2$-complex, the enzymatic activity of each subunit is stimulated by 1−2 orders of magnitude (*9*, *16*). This mutual activation

[†] This work was supported in part by the "National Project for Protein Structural and Functional Analysis" funded by the Ministry of Education, Culture, Sports, Science and Technology of Japan.

[‡] Coordinates have been deposited in the Protein Data Bank as entries 1V7Y and 1WQ5.

* To whom correspondence should be addressed: RIKEN Harima Institute, 1-1-1 Kouto, Mikazuki-cho, Sayo-gun, Hyogo 679-5148, Japan. Telephone: 81-791-58-2937. Fax: 81-791-58-2917. E-mail: yutani@spring8.or.jp.

[§] Osaka University.

[||] Kyoto University.

[⊥] RIKEN Harima Institute.

[@] The University of Tokushima.

10.1021/bi047927m CCC: $30.25
Published on Web 12/31/2004

of the two subunits is suspected to come from conformational changes in the subunits upon formation of the complex (*12*, *17*). Therefore, tryptophan synthase is an excellent model for studying the relation between the activation of a function and conformational change in the protein. In 1988, the three-dimensional structure of the tryptophan synthase $\alpha_2\beta_2$-complex from *Salmonella typhimurium* (*St*$\alpha_2\beta_2$-complex)[1] was determined by X-ray crystallography (*18*). Furthermore, the crystal structures of the *St*$\alpha_2\beta_2$-complex with allosteric cations and/or ligands have been reported (*19*−*25*). These reports provide valuable information for understanding the allosteric mechanism of tryptophan synthase. To elucidate the structural basis of the mutual activation, it is necessary to determine the structures of the α- and β_2-subunits alone and to identify the conformational changes upon formation of the $\alpha_2\beta_2$ complex. Recently, the structures of the tryptophan synthase α-subunit alone (*Pf*α-subunit) (*26*) and the β_2-subunit alone (*Pf*β_2-subunit) (*27*) from hyperthermophile *Pyrococcus furiosus* have been reported. However, the structures of the subunits alone from the mesophiles have not yet been determined.

Thermodynamic analyses using titration calorimetry have revealed that the $\alpha_2\beta_2$-complex formation of tryptophan synthase from *Escherichia coli* couples with the folding (rearrangement) of the α-subunit monomer and/or β-subunit dimer (*17*), but the conformational change coupled with the subunit association is small in the $\alpha_2\beta_2$-complex from *P. furiosus* (*28*). In fact, the structures of the *Pf*α-subunit alone (*26*) and the *Pf*β_2-subunit alone (*27*) from *P. furiosus* have been reported to be similar to those of the respective α- and β-subunits in the complex from *S. typhimurium*. These results confirm the prediction from thermodynamic analysis that the conformational change due to complex formation is small in that from *P. furiosus*, although the structure of the complex from *P. furiosus* has not yet been determined. It is also expected from a thermodynamic point of view that the isolated structures of the α- and β_2-subunits of tryptophan synthase from mesophiles must be determined to elucidate whether the complex formation of the protein from mesophiles couples with the folding of each subunit.

We obtained a suitable crystal of the tryptophan synthase α-subunit (*Ec*α-subunit)[1] from *E. coli* for X-ray diffraction and determined its structure at 2.3 Å resolution. In this paper, we compare in detail the structures of the *Ec*α-subunit alone and the α-subunit in the *St*$\alpha_2\beta_2$-complex (*St*α-subunit). It was found that the formation of the $\alpha_2\beta_2$-complex induced large conformational changes in the loop region between strand 2 and helix 2. We will discuss the correlation of the conformational change with the stimulation of the α-subunit activity.

[1] Abbreviations: *Ec*α-subunit, tryptophan synthase α-subunit from *E. coli*; *Ec*β_2-subunit, tryptophan synthase β_2-subunit from *E. coli*; *Ec*β-subunit, tryptophan synthase monomer β-subunit from *E. coli*; *Ec*$\alpha_2\beta_2$-complex, tryptophan synthase $\alpha_2\beta_2$-complex from *E. coli*; *Ec*TSase, tryptophan synthase from *E. coli*; IGP, indole 3-glycerol phosphate; *Pf*α-subunit, tryptophan synthase α-subunit from *P. furiosus*; *Pf*β_2-subunit, tryptophan synthase β_2-subunit from *P. furiosus*; *Pf*β-subunit, tryptophan synthase monomer β-subunit from *P. furiosus*; *Pf*$\alpha_2\beta_2$-complex, tryptophan synthase $\alpha_2\beta_2$-complex from *P. furiosus*; *Pf*TSase, tryptophan synthase from *P. furiosus*; PLP, pyridoxal 5′-phosphate; rmsd, root-mean-square deviation; *St*α-subunit, tryptophan synthase α-subunit from *S. typhimurium*; *St*β_2-subunit, tryptophan synthase β_2-subunit from *S. typhimurium*; *St*β-subunit, tryptophan synthase monomer β-subunit from *S. typhimurium*; *St*$\alpha_2\beta_2$-complex, tryptophan synthase $\alpha_2\beta_2$-complex from *S. typhimurium*; *St*TSase, tryptophan synthase from *S. typhimurium*; *Tt*α-subunit, tryptophan synthase α-subunit from *T. thermophilus*.

EXPERIMENTAL PROCEDURES

Purification of the α*-Subunit from E. coli.* The *Ec*α-subunit was purified as described previously (*29*). The purified protein exhibited a single band on SDS−PAGE. The concentration of the protein was estimated from the absorbance at 278.5 nm, assuming $E^{1cm}_{1\%} = 4.4$ (*30*).

Crystallization and Data Collection. Crystals suitable for data collection were obtained at 288 K using the hanging-drop vapor diffusion method. A 1.0 μL aliquot of protein solution at a concentration of 20 mg/mL in 5 mM potassium phosphate buffer (pH 7) was mixed with an equal volume of reservoir solution [1.8 M ammonium sulfate and 0.1 M sodium cacodylate (pH 6.5)]. After 1 week, the crystals grew to full size (0.1 mm × 0.1 mm × 0.01 mm). The crystals were soaked in cryoprotectant [2.0 M ammonium sulfate, 0.1 M sodium cacodylate (pH 6.5), and 20% glycerol] for a few seconds and then were flash-cooled in a 100 K dry nitrogen stream. The X-ray diffraction data were collected at beamlines BL44XU and BL44B2, SPring-8, using the DIP6040 imaging plate detector. The data were processed using DENZO and SCALEPACK (*31*). The crystals belonged to space group *C*2, with two molecules in an asymmetric unit, a solvent content of 43.3%, and a specific volume (V_M) of 2.17 Å^3 Da^{-1} (*32*). The cell dimensions were as follows: $a = 156.77$ Å, $b = 44.63$ Å, $c = 71.72$ Å, and $\gamma = 96.5°$.

Structure Determination and Refinement. The structure was determined by the molecular replacement method using CNS (*31*). The full length of the α-subunit in the *St*$\alpha_2\beta_2$-complex [Protein Data Bank (PDB) entry 1BKS] (*18*) was used as an initial search model. Because the electron density map for residues 52−77 was not consistent with those of the reference structure, these residues were excluded from the reference molecule and the phases were then calculated to generate an unbiased electron density map. All refinements were carried out using CNS. The sigma-A-weighted composite omit map was calculated by CNS to reduce the model bias. The structure was visualized and modified using XtalView (*33*) and O (*34*). The refined model consisted of two molecules (Mol-A and Mol-B) in an asymmetric unit. Residues 1−56, 65−183, and 186−268 were identified in Mol-A, and residues 1−58, 64−183, and 186−268 were identified in Mol-B. The model geometry was analyzed with PROCHECK (*35*). The data collection and refinement statistics are summarized in Table 1. The final coordinates and the structure factors have been deposited in the Protein Data Bank (entries 1V7Y and 1WQ5).

Analysis for Sequences and Molecules. The multiple-sequence alignment among the *Ec*α-subunit, the *St*α-subunit (PDB entry 1BKS), the *Pf*α-subunit (PDB entry 1GEQ), and the α-subunit (*Tt*α-subunit) (PDB entry 1UJP) from *Thermus thermophilus* was carried out using CLUSTAL W (*36*). The secondary structures of all coordinates were defined by DSSP (*37*). LSQKB (*38*) supported by the program package CCP4 (*39*) was used for superposition of all the coordinates. The structures of Mol-A and Mol-B could be superimposed between equivalent Cα atoms of residues 1−56, 65−183,

Table 1: Data Collection and Refinement Statistics

Crystal Data Statistics	
X-ray source	SPring-8 BL44XU
detector	DIP 6040
wavelength (Å)	0.9
crystal-to-detector distance (mm)	360
exposure time (s)	5
data collection temperature (K)	100
no. of crystals per image	1/180
space group	*C*2
unit cell parameters	
a (Å)	156.77
b (Å)	44.63
c (Å)	71.72
β (deg)	96.46
resolution range (Å)[a]	49.86−2.30 (2.38−2.30)
no. of total reflections[a]	75855 (6988)
no. of unique reflections[a]	21699 (2079)
$\langle I/\sigma(I)\rangle$[a]	7.9 (3.85)
completeness (%)[a]	98 (94.2)
R_{merge} (%)[a]	0.116 (0.383)
redundancy[a]	3.5 (3.4)
no. of molecules per asymmetric unit	2
V_M (Å^3/Da)	2.17
Refinement Statistics	
resolution range (Å)[a]	49.86−2.30 (2.38−2.30)
σ cutoff (*F*)	0
R_{cryst} (%)[a,b]	18.5 (25.5)
R_{free} (%)[a,c]	24.8 (32.7)
no. of atoms	
no. of protein atoms	3943
no. of sulfate ions	13
no. of glycerol molecules	8
no. of water molecules	197
average *B*-factor (Å^2)	
all	33.5
proteins	30.4
sulfate ions	70
glycerol molecules	53.8
water molecules	35.2
rmsd for bonds (Å)	0.008
rmsd for angles (deg)	1.4
Ramachandran plot (%)	
most favored	92.2
additional allowed	7.3
generously allowed	0.5
disallowed	0

[a] Values in parentheses are for the highest-resolution shell. [b] R_{cryst} was calculated from the working set (95% of the data). [c] R_{free} was calculated from the test set (5% of the data).

and 186−268 in both subunits with a root-mean-square deviation (rmsd) of 0.9 Å. Two structures (PDB entries 1BKS and 1QOQ) of the α-subunits in the *St*$\alpha_2\beta_2$-complex without (*18*) and with a substrate, indole 3-glycerol phosphate (IGP) (*24*), respectively, were superimposed on equivalent Cα atoms of the *Ec*α-subunit (Mol-A). The Cα atoms in loop A (residues 52−77) and loop B (residues 178−192) were omitted for the calculation, because the structures of loops A and B were very different from each other in the *Ec*α-subunit alone and the *St*α-subunit in the *St*$\alpha_2\beta_2$-complex. The rmsd values of Cα atoms for the superimposed Mol-A without loops A and B on the *St*α-subunit were 0.96 and 0.81 Å for 1BKS and 1QOQ, respectively. The potential hydrogen bonds were examined using XtalView (*33*).

RESULTS

Overall Structure of the Tryptophan Synthase α*-Subunit Alone from E. coli.* The *Ec*α-subunit crystals belonged to space group *C*2, and eight molecules were contained in a unit cell. There were two molecules (Mol-A and Mol-B) in an asymmetric unit **(**Figure 1A). The overall fold of the *Ec*α-subunit alone was a $(\beta/\alpha)_8$-barrel first observed in a triose-phosphate isomerase (*40*). The helices and strands corresponding to canonical α/*β*-barrel elements have been consecutively numbered from 1 to 8. The structure of the *Ec*α-subunit alone had two extra α-helices, helix 0 and helix 8′, resulting in a total of 10 helices. Helix 0 and helix 8′ were located in the N-terminus and between strand 8 and helix 8, respectively (Figures 1B and 2). Two unique structures were observed in the structure of the *Ec*α-subunit alone. One was loop A (residues 52−77) between strand 2 and helix 2, and the other, loop B (residues 178−192), was between strand 6 and helix 6. Loop A was a long flexible loop that included an active site residue, Asp60. The *B*-factors of loop A and loop B in both molecules were larger than those of the other regions.

Mol-A and Mol-B in an asymmetric unit were connected in a unique style in which loop A of each molecule formed hydrogen bonds with residues near the active site of a partner molecule via sulfate anions, resulting in a dimeric form (Figure 1A). The electron densities of residues 57−64, 184, and 185 in Mol-A and residues 59−63, 184, and 185 in Mol-B were not clear.

Comparison of Amino Acid Sequences between the α*-Subunits from E. coli and S. typhimurium.* The number of amino acid residues for the *Ec*α-subunit and the *St*α-subunit is the same, 268, and the level of sequence identity between both proteins is 85% (Figure 2). All residues related to the catalytic function and interaction with the *β*-subunit are conserved in both α-subunits: catalytic residues (Glu49 and Asp60) (*29*, *41*), ligand pockets [Phe22, Tyr102, Tyr175, Leu177, Gly211, Gly213, Gly234, and Ser235, in 1BKS (*18*)], the residues that interacted with the phosphate moiety of IGP [Gly213, Gly234, and Ser235, in 1QOQ (*24*)], and the residues forming hydrogen bonds at the α- and *β*-subunit interface [Ser55, Asp56, Gln65, Asn104, Asn108, Val133, Glu134, Glu135, and Asn157, in 1BKS (Table 2)]. The residues in loop A of the *Ec*α-subunit consisting of 26 residues are highly conserved, where only two residues, Ile52 and Thr68, are replaced with Val and Asn in the *St*α-subunit, respectively. Two residues, Ala180 and Ala189, among 15 residues in loop B of the *Ec*α-subunit are changed to Ser and Gly, respectively, in the *St*α-subunit (Figure 2).

*Comparison of the Structures of the Ec*α*-Subunit Alone with the* α*-Subunit in the St*$\alpha_2\beta_2$*-Complex.* The structures of the *Ec*α-subunit and the *St*α-subunit were compared by superimposition of equivalent Cα atoms in both subunits (Figure 3). The rmsd profile of each residue between two α-subunits is shown in Figure 4. The large conformational differences between two molecules were detected for residues 52−77 and 178−192, corresponding to loop A and loop B, respectively, in the *Ec*α-subunit. In the *St*α-subunit, the region corresponding to residues 52−77 forms loop 2 (residues 52−61) and helix 2′ (residues 62−74) that are the lid of the TIM barrel and look like "the roof of the active site". In contrast, loop A of the *Ec*α-subunit was a long loop structure except for a short α-helix of four residues. Furthermore, loop A was bent toward the outside of the TIM barrel as if it opens a roof (Figure 3B). Several residues in loop A (residues 57−64 and 59−63 in Mol-A and Mol-B,

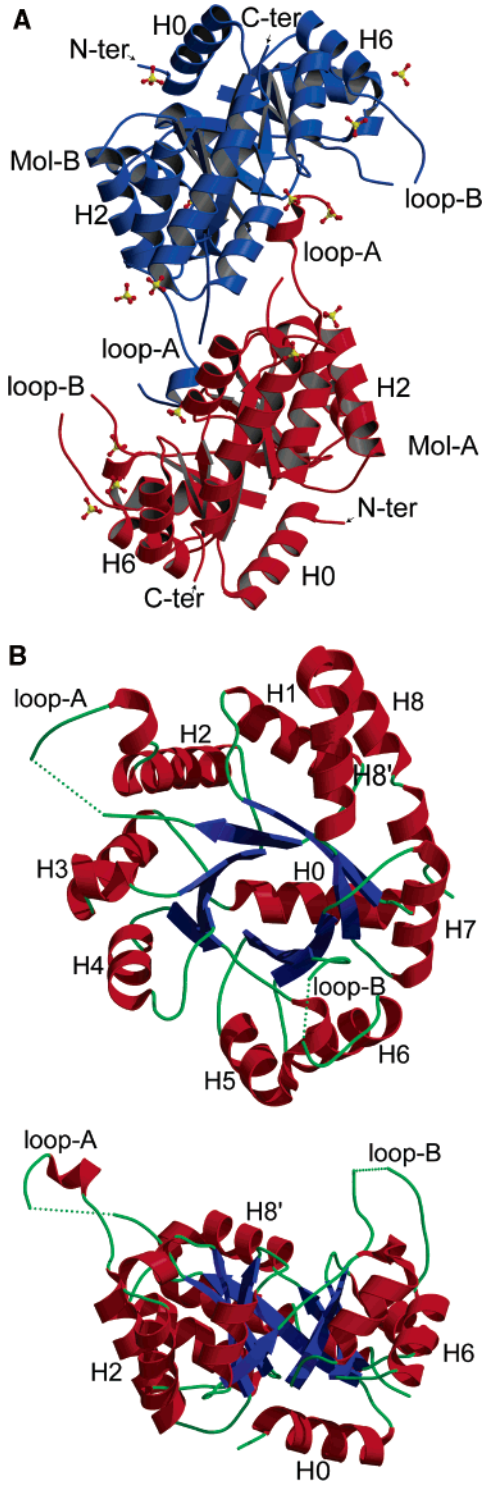

FIGURE 1: Schematic views of the structure of the *Ec*α-subunit alone. (A) Structures of two *Ec*α-subunits in an asymmetric unit. Mol-A and Mol-B are colored red and blue, respectively. Loop A consisting of residues 52−77 and loop B consisting of residues 178−192 protrude from the molecular surface. Sulfate anions are shown in a ball-and-stick representation. O atoms are red, and S atoms are yellow. The two molecules interact with each other through loop A and the sulfate anion. (B) Schematic views of the structure of Mol-A. The top and bottom panels are views from the C-terminal face of the α-subunit and from the side face of the barrel, respectively. The helices are depicted as red helical ribbons, β-strands as blue arrows, and other structures as green lines. Disordered regions in loop A and loop B are illustrated as green dotted lines. H0−H8 represent helices 0−8, respectively. The figure was prepared using MOLSCRIPT (*54*) and Raster3D (*55*).

respectively), including the catalytic residue, Asp60, were disordered in the crystal. Loop B of the *Ec*α-subunit was disordered at residues 184 and 185, while residues 178−189 of the *St*α-subunit corresponding to loop B were completely disordered. Small peaks 2−7 correspond to Lys109, Asn157, Pro192, Phe212, Gly234, and Asn246, respectively. Lys109 (peak 2) and Asn157 (peak 3) of the *Ec*α-subunit are located in helix 3 and loop 5, respectively. These residues are equivalent to Asn108 and Asn157 in the *St*α-subunit that form hydrogen bonds with residues of the β-subunit (Table 2). Pro192 (peak 4) is located in the C-terminus of loop B. Phe212 (peak 5) and Gly234 (peak 6) are located near residues (Gly213, Gly234, and Ser235) that bind with the phosphate of IGP through hydrogen bonds (*24*). This pattern of binding of a phosphate moiety by a hydrogen bond is called the "phosphate-binding motif" which is observed in many TIM barrel enzymes (*42*). In the case of the *Ec*α-subunit, Gly213 and Gly234 bind with the sulfate ion instead of IGP, which comes from the ammonium sulfate of the precipitants as the crystallization reagent (Figure 1A). Although the rmsd values for Phe212 (peak 5) and Gly234 (peak 6) between the *Ec*α-subunit and ligand-free *St*$\alpha_2\beta_2$-complex (1BKS) were 2.26 and 2.93 Å, respectively (Figure 4), those between the *Ec*α-subunit and IGP-bound *St*$\alpha_2\beta_2$-complex (1QOQ) were 0.29 Å for Phe212 and 0.78 Å for Gly234. The values were larger in the ligand-free *St*α-subunit (1BKS) than in the IGP-bound *St*α-subunit (1QOQ), suggesting that the deviations at residues 212 and 234 come from ligand (sulfate ion) binding. Asn246 (peak 7) is located in a turn between helix 8′ and helix 8. Asn246 of Mol-A and Gln243 of Mol-B interacted with a hydrogen bond through a water molecule. This suggests that the structural deviation at residue 246 comes from the intermolecular interaction between Mol-A and Mol-B in the crystal of the *Ec*α-subunit.

*Comparison of B-Factors between the Ec*α*-Subunit and the St*α*-Subunit.* To determine differences in the structural mobility between the two α-subunits, the changes in the *B*-factor of each residue were then calculated on the main chain between the *Ec*α-subunit alone (Mol-A) and the α-subunit in the *St*$\alpha_2\beta_2$-complex (1BKS). The *B*-factor of each protein was normalized to compare the *B*-factors between different proteins by eq 4 (*43*). The abnormally high *B*-factors in loop A and loop B were excluded for the normalization calculation.

$$B' = (B - \langle B \rangle)/\sigma(B) \qquad (4)$$

where B', B, $\langle B \rangle$, and $\sigma(B)$ represent the normalized *B*-factor, the *B*-factor of the main chain, the averaged *B*-factor of the main chains, and the standard deviation of the *B*-factors, respectively. Differences ($\Delta B'$) in the normalized *B*-factor between the *Ec*α-subunit and the α-subunit in the *St*$\alpha_2\beta_2$-complex are plotted for each residue in Figure 5. Four positive peaks appeared. The extremely large $\Delta B'$ (peak 1) of the residues corresponding to loop A in the *Ec*α-subunit indicates that loop A protruding from the molecular surface is more mobile than the corresponding residues of the *St*$\alpha_2\beta_2$-complex buried inside the molecule. The segments with positive peaks, the N-termini of helix 3, loop 4 (residues 129−136), and helix 5, are included in the regions at the subunit interface. All of the residues forming hydrogen bonds between the α- and the β-subunits in the *St*α-subunit (Table

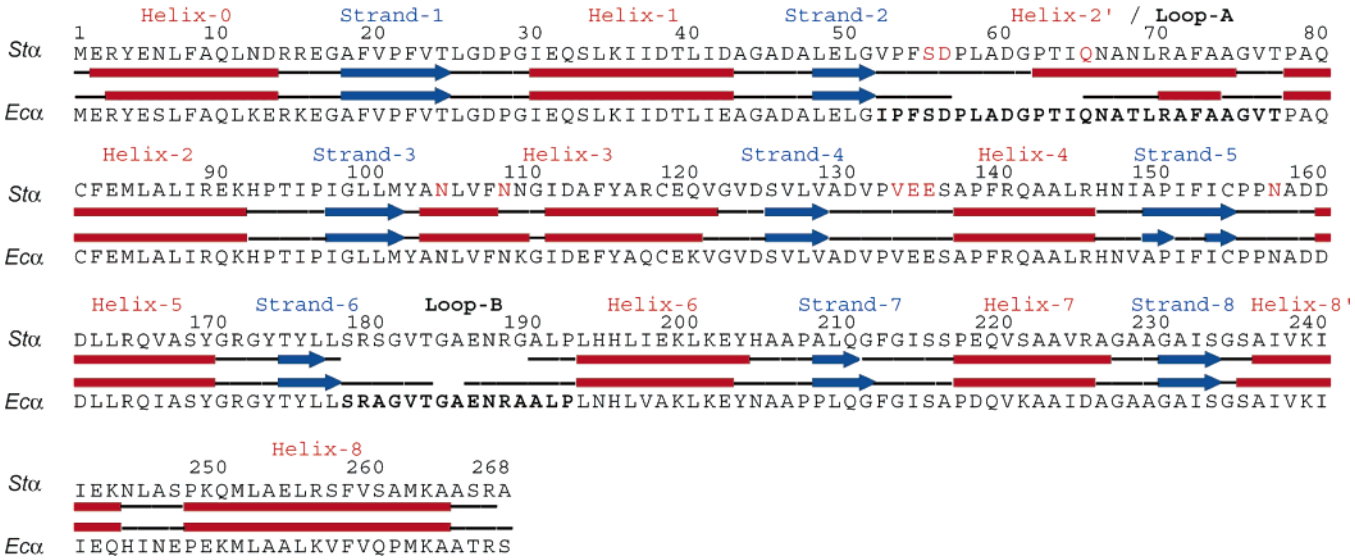

FIGURE 2: Sequence alignments with secondary structures of the *Ec*α-subunit and the *St*α-subunit. The first line represents the alias of the secondary segments named by Hyde et al. (*18*). The second line represents the sequence number of the α-subunits. The third and sixth lines represent amino acid sequences of the *St*α-subunit and the *Ec*α-subunit, respectively. The fourth and fifth lines represent the secondary structural elements of the *St*α-subunit (PDB entry 1BKS) and the *Ec*α-subunit (Mol-A), respectively, based on the secondary structure definition as established by DSSP (*37*). A red block, a blue arrow, a black bar, and a space represent the α-helix, the *β*-strand, the others, and a missing region, respectively. Red letters in the third line represent hydrogen-bonding residues of the *St*α-subunit with the *β*-subunit. Bold letters in the sixth line represent the residues of loop A or loop B of the *Ec*α-subunit.

Table 2: Hydrogen Bonds between the α-Subunit and *β*-Subunit in the *St*$\alpha_2\beta_2$-Complex[a]

α-subunit			*β*-subunit			hydrogen bond
structure[b]	residue	atom	structure[b]	residue	atom	distance (Å)
loop 2	Ser55	N	loop 8	Ile293	OE1	2.90
loop 2	Ser55	OG	loop 8	Ile294	N	3.06
loop 2	Asp56	OD1	helix 6	Lys167	N1	3.29
loop 2	Asp56	OD2	helix 6	Lys167	N1	2.95
helix 2′	Gln65	OE1	loop 5	Ser161	OG	2.71
helix 3	Asn104	ND2	loop 8	Gln288	NE2	2.91
helix 3	Asn104	ND2	loop 8	Gly292	O	2.73
helix 3	Asn104	OD1	loop 8	Ile278	N	2.71
helix 3	Asn108	OD1	loop 8	Arg275	NH2	2.57
loop 4	Val133	N	N-terminus	Gln19	OE1	2.85
loop 4	Glu134	OE1	N-terminus	Gln19	NE2	2.90
loop 4	Glu135	OE1	N-terminus	Tyr8	OH	2.81
loop 4	Glu135	OE2	N-terminus	Tyr8	OH	3.22
loop 4	Glu135	OE2	N-terminus	Met15	N	2.48
loop 5	Asn157	ND2	N-terminus	Ile20	O	3.14
loop 5	Asn157	ND2	loop 5′	Tyr181	OH	2.91

[a] The hydrogen bonds were obtained using the *St*$\alpha_2\beta_2$-complex (PDB entry 1BKS). [b] Structures of the hydrogen-bonding residues are indicated by secondary structure: loop 2 (residues 52−61), helix 2′ (residues 62−74), helix 3 (residues 103−121), loop 4 (residues 129−136), and loop 5 (residues 155−159) of the α-subunit and N-terminus (residues 1−23), loop 5 (residues 160−165), loop 5′ (residues 178−183), helix 6 (residues 166−177), and loop 8 (residues 257−310) of the *β*-subunit.

2) exhibit a positive $\Delta B'$ (Figure 5). Ser55, Asp56, and Gln65 are located in loop A in the *Ec*α-subunit (Figures 3B and 5). These results indicate that the residues located in loop A and in the α/*β*-subunit interface become more mobile in the isolated α-subunit.

DISCUSSION

We will discuss the conformational changes due to formation of the $\alpha_2\beta_2$-complex of tryptophan synthase using the obtained structure of the *Ec*α-subunit, assuming that the *St*$\alpha_2\beta_2$-complex with 92% of the sequence identical (85% for the α-subunit and 97% for the *β*-subunit) should have an overall structure similar to that of the *Ec*$\alpha_2\beta_2$-complex, because the structure of the *Ec*$\alpha_2\beta_2$-complex has not yet been determined.

Stabilization of Helix 2′ Due to Complex Formation. In loop A of the *Ec*α-subunit, the difference in amino acid sequences between the *Ec*α-subunit and the *St*α-subunit is only 2 among 26 residues (Figure 2). The secondary structure for residues 52−77 of loop A in the *Ec*α-subunit has been predicted to be CCTCCCCTCCCCSSSSSHHHSHTTCC and H?????TTTTTSSSSSHHHHHHH?SS using the methods of Garnier et al. (*44*) and Chou and Fasman (*45*, *46*), respectively. H, S, C, T, and ? represent the α-helix, *β*-strand, coil, *β*-reverse turn, and no prediction, respectively.

The short helix from residue 70 to 73 in loop A coincided well with the above predictions. However, the region (residues 62−69) forming helix 2′ in the *St*$\alpha_2\beta_2$-complex is not predicted to be a helix, suggesting that the sequence of residues in loop A does not have a strong propensity for helix. These residues in the $\alpha_2\beta_2$-complex form loop 2 and helix 2′ with a four-turn helix, which are stabilized by hydrophobic interactions and hydrogen bonds with the residues of both the α- and *β*-subunits (Table 2). This suggests that helix 2′ in the α-subunits from mesophiles cannot be maintained without interaction with the *β*-subunits. The protruding loop A in the *Ec*α-subunit alone is transferred to the lid of the TIM barrel and forms helix 2′ by undergoing a tight interaction with the *β*-subunit in the $\alpha_2\beta_2$-complex (Figure 6A,B). The structural change from loop A of the *Ec*α-subunit alone to helix 2′ of the complex must be performed by an induced-fit mode (*2*−*6*) coupled to an intermolecular interaction with the *β*-subunit.

*Active Form of the Ec*α*-Subunit Alone.* In the tryptophan biosynthesis pathway, there are three TIM barrel enzymes, phosphoribosyl anthranilate isomerase (PRAI), indole glycerol phosphate synthase (IGPS) (*47*), and the trypto-

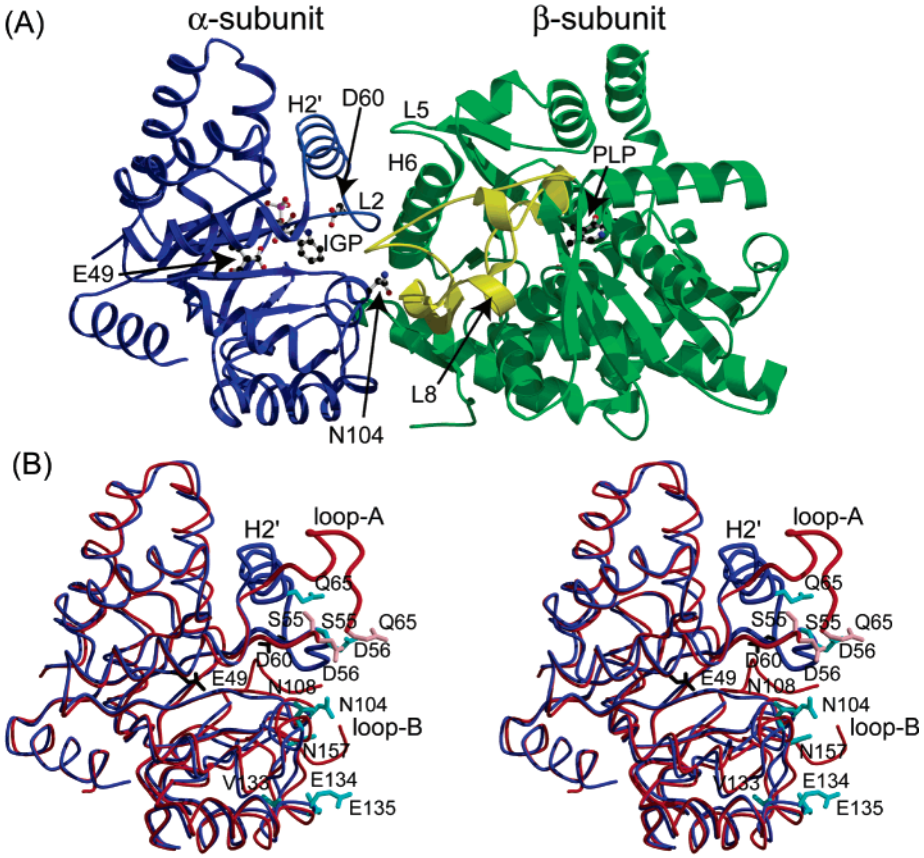

FIGURE 3: Schematic views of the *St*$\alpha_2\beta_2$-complex and the *Ec*α-subunit alone. (A) Structure of the *St*$\alpha_2\beta_2$-complex (PDB entry 1QOQ). Blue, green, and yellow represent the *St*α-subunit, the *St*β-subunit, and loop 8 in the *St*β-subunit, respectively. IGP and PLP bound in the *St*$\alpha_2\beta_2$-complex and the functionally important residues Glu49, Asp60, and Asn104 in the *St*α-subunit are represented by balls and sticks with an amino acid name by single-letter notation. (B) Schematic stereo drawing of superposition of the *Ec*α-subunit and the *St*α-subunit viewed from the same direction as the *St*$\alpha_2\beta_2$-complex in panel A. Red and blue represent the *Ec*α-subunit and the α-subunit in the *St*$\alpha_2\beta_2$-complex (PDB entry 1BKS), respectively. The hydrogen-bonding residues in the *St*α-subunit with the β-subunit and catalytic residues are represented as the cyan stick and black stick, respectively. The residues of the *Ec*α-subunit corresponding to the hydrogen-bonding residues in the *St*α-subunit are represented as pink sticks. The indications are the same as those in Figure 1. Disordered regions in loop A and loop B are not illustrated. The figure was produced with MOLSCRIPT (*54*) and Raster3D (*55*).

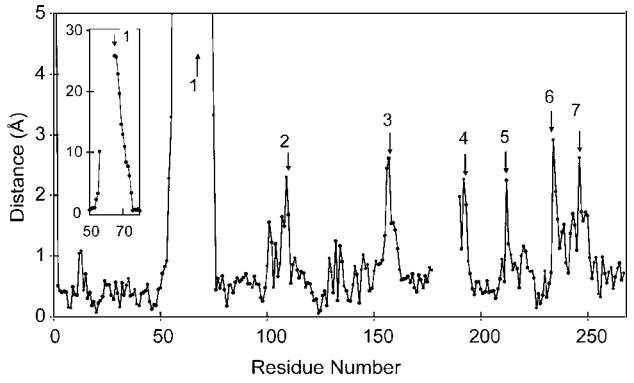

FIGURE 4: Root-mean-square deviations (angstroms) of Cα atoms between the *Ec*α-subunit alone and the *St*α-subunit (PDB entry 1BKS). Peaks 1−7 represent only discrimination marks for large differences.

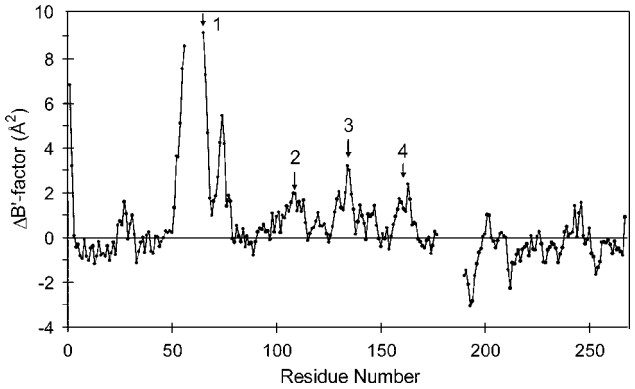

FIGURE 5: Differences in normalized *B*-factors (square angstroms) for the main chain atoms vs residue number between the *Ec*α-subunit and the *St*α-subunit. The Δ*B*′ factor means subtraction of values of the α-subunit in the *St*$\alpha_2\beta_2$-complex (PDB entry 1BKS) from those of the *Ec*α-subunit (Mol-A). Arrows indicate residues in the *Ec*α-subunit corresponding to hydrogen-bonding residues with the β-subunit in the *St*α-subunit.

phan synthase α-subunit (*18*), which have a common phosphate-binding motif on loop 7, loop 8, and helix 8′, respectively (*42*, *47*−*51*). These TIM barrel enzymes have a flexible long loop (more than 10 residues) that is inserted between strand 6 and helix 6 (*47*, *52*). In many TIM barrel enzymes, it is found that the flexible long loops play a common role in catalytic functions (*42*, *47*−*52*). In the case of tryptophan synthase, the α-subunit has loop 2 and an additional α-helix (helix 2′) between strand 2 and helix 2. Loop 2 and helix 2′ are crucial for the catalytic function of the α-subunit, including an active site residue, Asp60 (*19*, *23*, *24*), and important residues interacting with the β-subunit. The largest change observed in the structure of the *Ec*α-subunit alone occurred in this region.

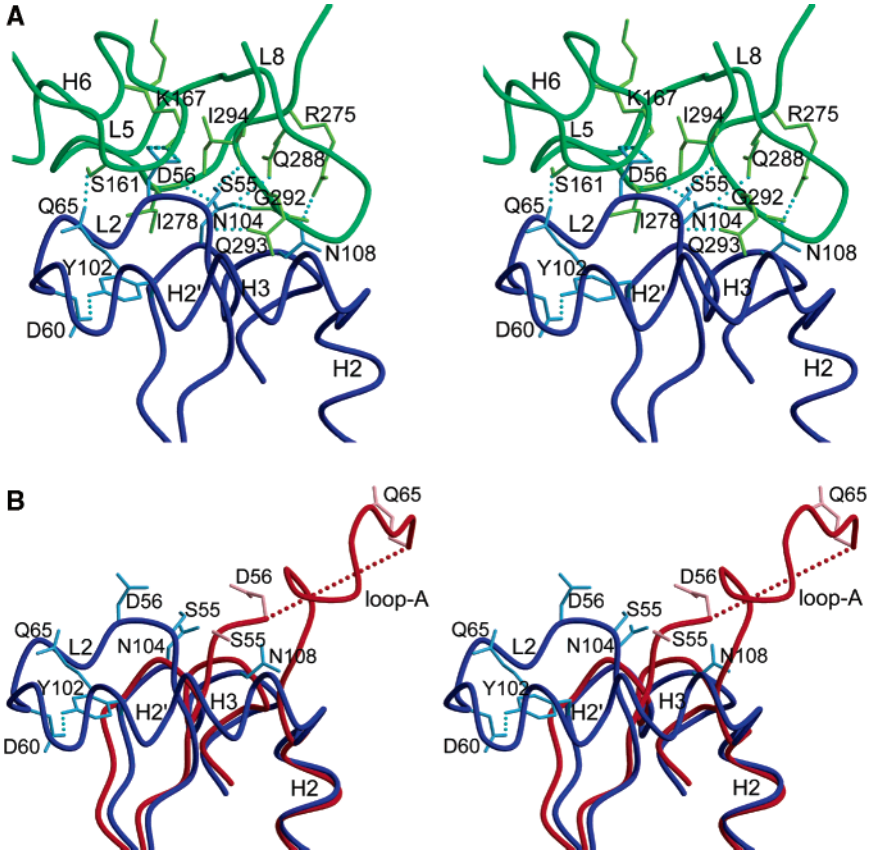

FIGURE 6: Schematic stereoview near helix 2′ of the *St*$\alpha_2\beta_2$-complex and the *Ec*α-subunit alone. Red, blue, and green wires represent the *Ec*α-subunit, the *St*α-subunit, and the *St*β-subunit, respectively. (A) Interaction between the α-subunit and β-subunit in the *St*$\alpha_2\beta_2$-complex. The hydrogen-bonding residues (Table 2) between the α- and β-subunits in the *St*$\alpha_2\beta_2$-complex (PDB entry 1BKS) are represented as sky blue sticks in the α-subunit and light green sticks in the β-subunit. Hydrogen bonds between the *St*α-subunit and the *St*β-subunit are drawn using cyan dotted lines. (B) Superposition of the *Ec*α-subunit and the *St*α-subunit. The disordered region in loop A is drawn as a dotted line. The residues of the *Ec*α-subunit corresponding to the hydrogen-bonding residues in the *St*α-subunit are represented as pink sticks. This figure was produced using MOLSCRIPT (*54*) and Raster3D (*55*).

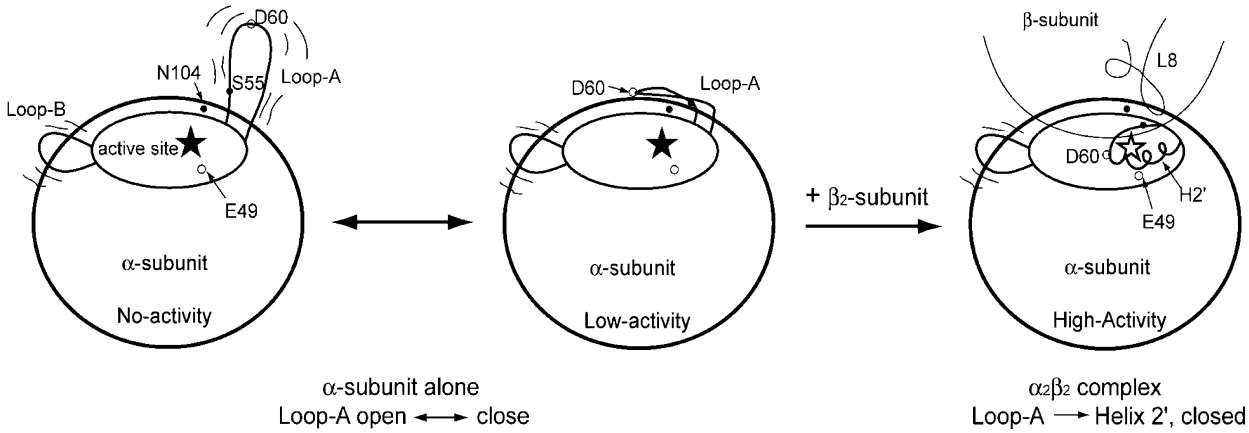

FIGURE 7: Scheme for forming the $\alpha_2\beta_2$-complex of the *Ec*α-subunit in the presence of the β-subunit. The left two molecules represent the states of the α-subunit alone in solution. In the absence of the β-subunit, loop A including Asp60 is in equilibrium between the opened and closed forms. The open and closed forms are inactive and active, respectively. In the presence of the β-subunit, only the α-subunit in the closed state can form a complex with the β-subunit. Finally, the closed form can construct the $\alpha_2\beta_2$-complex form, in which the conformation with the correct active site is stabilized.

The most important catalytic base of the *Ec*α-subunit is Glu49 (*29*, *53*), and Asp60 is a second catalytic base (*41*, *53*). In the crystal form of the *Ec*α-subunit alone, Asp60 is far from the position of Asp60 in the *St*$\alpha_2\beta_2$-complex (Figure 6B), indicating that the *Ec*α-subunit alone cannot carry out a catalytic function. However, the *Ec*α-subunit alone in solution has an enzymatic activity that is less efficient. The $\alpha_2\beta_2$-complex exhibits an α activity ~30 times higher than that of the isolated α-subunit (*9*, *12*, *16*). Therefore, it is expected that the *Ec*α-subunit in solution is in equilibrium between the active and inactive forms. As illustrated in Figure 7, in the absence of the β-subunit, loop A including Asp60 can be suggested to be in equilibrium between the opened and closed forms. The open form is inactive and is equivalent to the crystal structure of the *Ec*α-subunit alone or is an ensemble of flexible loop structures in solution. In the closed

Table 3: Sequence Identity among the *Pf*α-Subunit, *Tt*α-Subunit, *St*α-Subunit, and *Ec*α-Subunit[a]

	*Pf*α	*Tt*α	*St*α	*Ec*α
*Pf*α (248)	−	37%/40%	33%/46%	33%/46%
*Tt*α (271)	37%/40%	−	27%/46%	26%/46%
*St*α (268)	33%/46%	27%/46%	−	85%/93%
*Ec*α (268)	33%/46%	26%/46%	85%/93%	−

[a] The comparison of the level of sequence identity between two α-subunits of four species. The values to the left and right of the slant represent the levels of sequence identity (%) calculated for the whole molecules and for only helix 2′, respectively.

form, loop A folds to the inside of the TIM barrel and the activity appears. The ratio of the closed form would be extremely low in the absence of the β-subunit, resulting in low activity. Finally, in the presence of the β-subunit, the closed form can construct the $\alpha_2\beta_2$-complex form, including helix 2′, in which the conformation around the active site is stabilized by many interactions with residues in the α- and β-subunits (Table 2 and Figure 6A).

*Comparison of Structures of the Ec*α*-Subunit with* α*-Subunits from Thermophiles.* The available coordinates of the α-subunits alone from the hyperthermophile *P. furiosus* (*Pf*α-subunit) (*26*) and the extreme thermophile *T. thermophilus* (*Tt*α-subunit) have been deposited in the PDB. The overall structures of the two thermophiles are essentially similar to that of the *Ec*α-subunit except for the loop A region. The structures of the *Pf*α-subunit and the *Tt*α-subunit corresponding to loop A in the *Ec*α-subunit alone consist of loop 2 and helix 2′ like that of the α-subunit in the *St*$\alpha_2\beta_2$-complex. Why can the thermophile proteins construct helix 2′ in the absence of the β-subunit? The number of total residues is 268, 271, and 248 in the *Ec*α-subunit, the *Tt*α-subunit, and the *Pf*α-subunit, respectively. The sequence of the helix 2′ region for the *St*α-subunit was more similar to those of the thermophile proteins than that of the whole sequence (Table 3). The helix propensities at the N-terminal part of helix 2′ of the thermophile proteins were higher than those of mesophile proteins, which were calculated using the parameters obtained by Chou and Fasman (*46*). The numbers of residues in helix 2′ involved in the hydrogen bonds or ion pairs with other regions within the α-subunits were one (Arg70), three (Arg64, Ser66, and Glu67), and six (Lys49, Glu53, Ser54, His55, Arg57, and Asn61) for the *St*α-subunit, the *Tt*α-subunit, and the *Pf*α-subunit, respectively. These hydrogen bonds and ion pairs should contribute to stabilization of helix 2′. Therefore, the stability of helix 2′ might be the highest in the *Pf*α-subunit and lowest in the *St*α-subunit even in the complex form among the three α-subunits. These results suggest that the helix propensity of the residues and stability of the helical structure determine whether helix 2′ can be involved in the isolated α-subunit. In other words, acquisition of helix 2′ in isolated α-subunits from thermophiles may come from the necessity for enhancing the stability of the proteins. In fact, the denaturation temperature of the *Pf*α-subunit alone is higher by 32 °C than that of the *Ec*α-subunit (*28*).

The conformational changes in the α-subunit due to formation of the $\alpha_2\beta_2$-complex might be smaller in the thermophiles than in the mesophiles, because helix 2′ is already constructed in the isolated α-subunits of the thermophile proteins. This speculation agrees with the results of the thermodynamic analyses upon association of the α- and β-subunits from *E. coli* and *P. furiosus*. From the analyses of titration calorimetry, it has been reported that the folding of many residues is coupled to the α/β-subunit association of the *Ec*TSase (*17*), but the number of residues of local folding is slight for the association of the *Pf*TSase (*28*). These experiments resulted in confirming the prediction of the conformational changes from the thermodynamic analysis. Finally, we can conclude that the α/β-subunit association occurs by an induced fit mode with large conformation changes in *Ec*TSase and *St*TSase from mesophiles and a lock and key mode in *Pf*TSase from the thermophiles (*28*).

NOTE ADDED IN PROOF

Recently, Jeong et al. (*56*) have reported that the electron densities of residues 55−75, which corresponds to Helix-2′ of the *Ec*α-subunit, are not visible.

REFERENCES

1. Goh, C. S., Milburn, D., and Gerstein, M. (2004) Conformational changes associated with protein−protein interactions, *Curr. Opin. Struct. Biol. 14*, 104−109.
2. Koshland, D. E. J. (1958) Protein structure and enzyme action, *Proc. Natl. Acad. Sci. U.S.A. 44*, 98−104.
3. Yengo, C. M., De La Cruz, E. M., Chrin, L. R., Gaffney, D. P., II, and Berger, C. L. (2002) Actin-induced closure of the actin-binding cleft of smooth muscle myosin, *J. Biol. Chem. 277*, 24114−24119.
4. Conibear, P. B., Bagshaw, C. R., Fajer, P. G., Kovacs, M., and Malnasi-Csizmadia, A. (2003) Myosin cleft movement and its coupling to actomyosin dissociation, *Nat. Struct. Biol. 10*, 831−835.
5. Evdokimov, A. G., Phan, J., Tropea, J. E., Routzahn, K. M., Peters, H. K., Pokross, M., and Waugh, D. S. (2003) Similar modes of polypeptide recognition by export haperones in flagellar biosynthesis and type III secretion, *Nat. Struct. Biol. 10*, 789−793.
6. Kimple, R. J., Kimple, M. E., Betts, L., Sondek, J., and Siderovski, D. P. (2002) Structural determinants for GoLoco-induced inhibition of nucleotide release by Gα subunits, *Nature 416*, 878−881.
7. Tsai, C. J., Kumar, S., Ma, B., and Nussinov, R. (1999) Folding funnels, binding funnels, and protein function, *Protein Sci. 8*, 1181−1190.
8. James, L. C., Roversi, P., and Tawfik, D. S. (2003) Antibody multispecificity mediated by conformational diversity, *Science 299*, 1362−1367.
9. Miles, E. W. (1979) Tryptophan synthase: Structure, function, and subunit interaction, *Adv. Enzymol. Relat. Areas Mol. Biol. 49*, 127−186.
10. Miles, E. W. (1986) Pyridoxal phosphate enzymes catalyzing β-elimination and β-replacement reactions, in *Pyridoxal Phosphate: Chemical, Biochemical, and Medical Aspects, Part B* (Dolphin, D., Poulson, R., and Avramovic, O., Eds.) pp 253−310.
11. Miles, E. W. (1991) Structural basis for catalysis by tryptophan synthase, *Adv. Enzymol. Relat. Areas Mol. Biol. 64*, 93−172.
12. Miles, E. W. (1995) Tryptophan synthase. Structure, function, and protein engineering, *Subcell. Biochem. 24*, 207−254.
13. Miles, E. W., Ahmed, S. A., Hyde, C. C., Kayastha, A. M., Yang, X.-J., Ruvinov, S. B., and Lu, Z. (1994) Tryptophan synthase, in *Molecular aspects of enzyme catalysis* (Fukui, T., and Soda, K., Eds.) pp 127−146, Kodansha, Ltd., Tokyo, Japan, and VCH Publishers, New York.
14. Miles, E. W., Rhee, S., and Davies, D. R. (1999) The MOLECULAR basis of substrate channeling, *J. Biol. Chem. 274*, 12193−12196.
15. Pan, P., Woehl, E., and Dunn, M. F. (1997) Protein architecture, dynamics and allostery in tryptophan synthase channeling, *Trends Biochem. Sci. 22*, 22−27.
16. Yanofsky, C., and Crawford, I. P. (1972) Tryptophan synthase, *Enzymes (3rd Ed.) 8*, 1−31.

17. Hiraga, K., and Yutani, K. (1996) A thermodynamic analysis of conformational change due to the $\alpha_2\beta_2$ complex formation of tryptophan synthase, *Eur. J. Biochem. 240*, 63−70.
18. Hyde, C. C., Ahmed, S. A., Padlan, E. A., Miles, E. W., and Davies, D. R. (1988) Three-dimensional structure of the tryptophan synthase $\alpha_2\beta_2$ multienzyme complex from *Salmonella typhimurium*, *J. Biol. Chem. 263*, 17857−17871.
19. Rhee, S., Parris, K. D., Ahmed, S. A., Miles, E. W., and Davies, D. R. (1996) Exchange of K^+ or Cs^+ for Na^+ induces local and long-range changes in the three-dimensional structure of the tryptophan synthase $\alpha_2\beta_2$ complex, *Biochemistry 35*, 4211−4221.
20. Rhee, S., Parris, K. D., Hyde, C. C., Ahmed, S. A., Miles, E. W., and Davies, D. R. (1997) Crystal structures of a mutant (βK87T) tryptophan synthase $\alpha_2\beta_2$ complex with ligands bound to the active sites of the α- and β-subunits reveal ligand-induced conformational changes, *Biochemistry 36*, 7664−7680.
21. Rhee, S., Miles, E. W., Mozzarelli, A., and Davies, D. R. (1998) Cryocrystallography and microspectrophotometry of a mutant (αD60N) tryptophan synthase $\alpha_2\beta_2$ reveals allosteric roles of αAsp60, *Biochemistry 37*, 10653−10659.
22. Rhee, S., Miles, E. W., and Davies, D. R. (1998) Cryocrystallography of a true substrate, indole-3-glycerol phosphate, bound to a mutant (αD60N) tryptophan synthase $\alpha_2\beta_2$ complex reveals the correct orientation of active site αGlu49, *J. Biol. Chem. 273*, 8553−8555.
23. Schneider, T. R., Gerhardt, E., Lee, M., Liang, P. H., Anderson, K. S., and Schlichting, I. (1998) Loop closure and intersubunit communication in tryptophan synthase, *Biochemistry 37*, 5394−5406.
24. Weyand, M., and Schlichting, I. (1999) Crystal structure of wild-type tryptophan synthase complexed with the natural substrate indole-3-glycerol phosphate, *Biochemistry 38*, 16469−16480.
25. Sachpatzidis, A., Dealwis, C., Lubetsky, J. B., Liang, P. H., Anderson, K. S., and Lolis, E. (1999) Crystallographic studies of phosphonate-based α-reaction transition-state analogues complexed to tryptophan synthase, *Biochemistry 38*, 12665−12674.
26. Yamagata, Y., Ogasahara, K., Hioki, Y., Lee, S. J., Nakagawa, A., Nakamura, H., Ishida, M., Kuramitsu, S., and Yutani, K. (2001) Entropic stabilization of the tryptophan synthase α-subunit from a hyperthermophile, *Pyrococcus furiosus*. X-ray analysis and calorimetry, *J. Biol. Chem. 276*, 11062−11071.
27. Hioki, Y., Ogasahara, K., Lee, S. J., Ma, J., Ishida, M., Yamagata, Y., Matsuura, Y., Ota, M., Ikeguchi, M., Kuramitsu, S., and Yutani, K. (2004) The crystal structure of the tryptophan synthase β_2 subunit from the hyperthermophile *Pyrococcus furiosus*. Investigation of stabilization factors, *Eur. J. Biochem. 271*, 2624−2635.
28. Ogasahara, K., Ishida, M., and Yutani, K. (2003) Stimulated interaction between α and β subunits of tryptophan synthase from hyperthermophile enhances its thermal stability, *J. Biol. Chem. 278*, 8922−8928.
29. Yutani, K., Ogasahara, K., Tsujita, T., Kanemoto, K., Matsumoto, M., Tanaka, S., Miyashita, T., Matsushiro, A., Sugino, Y., and Miles, E. W. (1987) Tryptophan synthase α subunit glutamic acid 49 is essential for activity. Studies with 19 mutants at position 49, *J. Biol. Chem. 262*, 13429−13433.
30. Ogasahara, K., Yutani, K., Suzuki, M., Sugino, Y., Nakanishi, M., and Tsuboi, M. (1980) State of Tyr49 in a mutant tryptophan synthase α-subunit substituted at position 49, *J. Biochem. 88*, 1733−1738.
31. Otwinowski, Z., and Minor, W. (1997) Processing of X-ray diffraction data collected in oscillation mode, *Methods Enzymol. 276*, 307−326.
32. Matthews, B. W. (1968) Solvent content of protein crystals, *J. Mol. Biol. 33*, 491−497.
33. McRee, D. E. (1999) XtalView/Xfit: A versatile program for manipulating atomic coordinates and electron density, *J. Struct. Biol. 125*, 156−165.
34. Jones, T. A., Zou, J. Y., Cowan, S. W., and Kjeldgaard, M. (1991) Improved methods for building protein models in electron density maps and the location of errors in these models, *Acta Crystallogr. A47*, 110−119.
35. Roman, A., Laskowski, M. W. M., Moss, D. S., and Thornton, J. M. (1993) PROCHECK: A program to check the stereochemical quality of protein structures, *J. Appl. Crystallogr. 26*, 283−291.
36. Thompson, J. D., Higgins, D. G., and Gibson, T. J. (1994) CLUSTAL W: Improving the sensitivity of progressive multiple sequence alignment through sequence weighting, position-specific gap penalties and weight matrix choice, *Nucleic Acids Res. 22*, 4673−4680.
37. Kabsch, W., and Sander, C. (1983) Dictionary of protein secondary structure: Pattern recognition of hydrogen-bonded and geometrical features, *Biopolymers 22*, 2577−2637.
38. Kabsch, W. (1976) A solution for the best rotation to relate two sets of vectors, *Acta Crystallogr. A32*, 922−923.
39. Collaborative Computational Project, No. 4 (1994) The CCP4 Suite: Programs for Protein Crystallography, *Acta Crystallogr. D50*, 760−763.
40. Banner, D. W., Bloomer, A., Petsko, G. A., Phillips, D. C., and Wilson, I. A. (1976) Atomic coordinates for triose phosphate isomerase from chicken muscle, *Biochem. Biophys. Res. Commun. 72*, 146−155.
41. Nagata, S., Hyde, C. C., and Miles, E. W. (1989) The α subunit of tryptophan synthase. Evidence that aspartic acid 60 is a catalytic residue and that the double alteration of residues 175 and 211 in a second-site revertant restores the proper geometry of the substrate binding site, *J. Biol. Chem. 264*, 6288−6296.
42. Wilmanns, M., Hyde, C. C., Davies, D. R., Kirschner, K., and Jansonius, J. N. (1991) Structural conservation in parallel β/α-barrel enzymes that catalyze three sequential reactions in the pathway of tryptophan biosynthesis, *Biochemistry 30*, 9161−9169.
43. Smith, D. K. (2003) Improved amino acid flexibility parameters, *Protein Sci. 12*, 1060−1072.
44. Garnier, J., Osguthorpe, D. J., and Robson, B. (1978) Analysis of the accuracy and implications of simple methods for predicting the secondary structure of globular proteins, *J. Mol. Biol. 120*, 97−120.
45. Chou, P. Y., and Fasman, G. D. (1974) Prediction of protein conformation, *Biochemistry 13*, 222−245.
46. Chou, P. Y., and Fasman, G. D. (1978) Prediction of the secondary structure of proteins from their amino acid sequence, *Adv. Enzymol. Relat. Areas Mol. Biol. 47*, 45−148.
47. Priestle, J. P., Grutter, M. G., White, J. L., Vincent, M. G., Kania, M., Wilson, E., Jardetzky, T. S., Kirschner, K., and Jansonius, J. N. (1987) Three-dimensional structure of the bifunctional enzyme N-(5′-phosphoribosyl)anthranilate isomerase-indole-3-glycerol-phosphate synthase from *Escherichia coli*, *Proc. Natl. Acad. Sci. U.S.A. 84*, 5690−5694.
48. Nagano, N., Hutchchinson, E. G., and Thornton, J. M. (1999) Barrel structures in proteins: Automatic identification and classification including a sequence analysis of TIM barrels, *Protein Sci. 8*, 2072−2084.
49. Petsko, G. A. (2000) Enzyme evolution. Design by necessity, *Nature 403*, 606−607.
50. Lang, D., Thoma, R., Henn-Sax, M., Sterner, R., and Wilimanns, M. (2000) Structural evidence for evolution of the β/α barrel scaffold by gene duplication and fusion, *Science 289*, 1546−1550.
51. Nagano, N., Orengo, C. A., and Thornton, J. M. (2002) One fold with many functions: The evolutionary relationships between TIM barrel families based on their sequences, structures and functions, *J. Mol. Biol. 321*, 741−765.
52. Wise, E. L., and Rayment, I. (2004) Understanding the importance of protein structure to Nature's routes for divergent evolution in TIM barrel enzymes, *Acc. Chem. Res. 37*, 149−158.
53. Miles, E. W., McPhie, P., and Yutani, K. (1988) Evidence that glutamic acid 49 of tryptophan synthase α subunit is a catalytic residue. Inactive mutant proteins substituted at position 49 bind ligands and transmit ligand-dependent to the β subunit, *J. Biol. Chem. 263*, 8611−8614.
54. Kraulis, P. J. (1991) MOLSCRIPT: A program to produce both detailed and schematic plots of protein structures, *J. Appl. Crystallogr. 24*, 946−950.
55. Bacon, D. J., and Anderson, W. F. (1988) A fast algorithm for rendering space-filling molecule pictures, *J. Mol. Graphics 6*, 219−220.
56. Jeong, M. S., Jeong, J. K., Lim, W. K., and Jang, S. B. (2004) Structure of wild-type and P28L/Y173F tryptophan synthase α-subunits from *Escherichia coli*. *Biochem. Biophys. Res. Commun. 323*, 1257−1264.

BI047927M